

Measurement Study and Transmission for In-vehicle Power Line Communication

M. Mohammadi, L. Lampe, M. Lok, S. Mirabbasi, M. Mirvakili, R. Rosales, and P. van Veen
Department of Electrical and Computer Engineering, University of British Columbia, Canada

Abstract—In-vehicle power line communication (PLC) holds great promises as an enabler of in-vehicle communication without increasing weight, volume, or cost of the wiring harnesses. In this paper, we join a few recent works and present channel measurements for a specific compact car. We discuss and compare our measurement results with those obtained in previous campaigns. Furthermore, we evaluate our measurements from the viewpoint of high connectivity. That is, we are interested in the suitability of PLC for applications that require a reliable link from any node to any other node at any time. Perhaps not surprisingly, we find that advanced transmission techniques such as multihop or frequency diversity are necessary to achieve this goal.

I. INTRODUCTION

The number of electronic systems in vehicles grows at an exponential pace [1]. The main purpose of these systems is to assist the driver to control the vehicle and to facilitate convenience functionalities such as entertainment and communication systems. The fast proliferation of in-vehicle electronics also increases the data traffic generated within the vehicle. To support this traffic, a considerable amount of additional wires solely dedicated to communication purposes are needed. These wires contribute notably to weight, volume, complexity, and cost of the wiring harness in a vehicle. Please refer to the excellent survey articles [1], [2] for an extensive discussion of automotive data networks, their applications, and problems associated with the increasing number of wires.

In-vehicle power line communication (PLC), i.e., the re-use of in-vehicle power lines for data communication, is a promising alternative that avoids the problems that come with extra wires for communication purposes. Although in-vehicle PLC is not a new idea (cf. e.g. [3]–[5]), it seems to enjoy a renewed interest, likely fostered by a green-shift in the automotive industry and maturing of PLC technology. For example, Ford Motor Company expects to “reduce the weight of a vehicle by more than 100 pounds through the elimination of wires” and identifies PLC as an enabler “to make vehicles lighter, less expensive to build and easier to add or remove electronic components” [6]. Also quite a few recent publications have been concerned with in-vehicle PLC, e.g. [7]–[11].

This paper is also dedicated to the problem of in-vehicle PLC and its purpose is twofold. First, we present and discuss a considerable number of channel measurements that have been made in a 2006 Pontiac Solstice. The Solstice is a small sports car from the Pontiac division of General Motors (GM) and it has the dimensions and electronic features typical for many compact cars by GM and other auto-makers. With our measurement results we intend to contribute to a better understanding and eventual modeling of the in-vehicle PLC channel, and to compare with and complement results for other car models (presumably by PSA Peugeot Citroën) presented in [10]. In this context, we also plan to establish a comprehensive online

This work was supported in part by the AUTO21 Network of Centres of Excellence, the National Sciences and Engineering Research Council (NSERC) of Canada, and Partners for the Advancement of Collaborative Engineering Education (PACE) program.

data base of in-vehicle channel measurements, and we have already made the full set of our measurement data reported here available in [12]. The second purpose of this paper is to investigate whether and how PLC is able to support communication for safety-critical components (e.g., “X-by-wire” solutions, in which electrical and electronic systems replace mechanical or hydraulic ones). That is, (i) we are interested to what extent PLC can connect two arbitrary nodes in the vehicle at any time and (ii) we focus on simple and robust transceiver technology for low-speed communication of say below 1 Mbps (suitable for Class A-C networks [2]). In this regard, our work differs from most other recent works [7]–[9] which focus on high-speed communication. Because of this second goal, (i) we consider a large number of different locations for transmitter and receiver nodes as well as different states of the car electronics and (ii) we perform measurements for a wide range of possible frequencies from about 500 kHz to 100 MHz. It will become apparent from our results that for high connectivity in an in-vehicle PLC network either frequency diversity or multihop transmission is mandatory. We thus provide one design example of the former class, which illustrates the effectiveness of advanced signal processing for PLC in vehicles. Finally, we note that while in this paper we concentrate on results for channel transfer function, the study of the in-vehicle noise environment [5], [7], [11] is subject of ongoing and future work.

The remainder of this paper is organized as follows. In Section II we will briefly introduce the measurement setup, and the measurement results are presented and discussed in Section III. In Section IV, we proceed with a statistical evaluation of the results, which will also lead us to a design example for a suitable communication system. Finally, Section V concludes this paper.

II. MEASUREMENT SETUP

In this section, we provide details about the measurement setup and some basic theoretical background necessary for the evaluation of the measurement results.

A. VNA Measurements

We consider the in-vehicle power lines used for data transmission (note that the chassis is the return path) as a two-port network between the transmitter and receiver devices. This two-port network is characterized using the scattering parameters (S -parameters) [13], which relate the incident (a_1, a_2) and reflected (b_1, b_2) waves at the input and output of the network as

$$\begin{bmatrix} b_1 \\ b_2 \end{bmatrix} = \mathbf{S} \begin{bmatrix} a_1 \\ a_2 \end{bmatrix}$$

using the scattering matrix

$$\mathbf{S} = \begin{bmatrix} S_{11} & S_{12} \\ S_{21} & S_{22} \end{bmatrix}.$$

We note that the S -parameters depend on the signal frequency f (we do make this dependency explicit for the sake of brevity). The use of S -parameters allows convenient measurements using

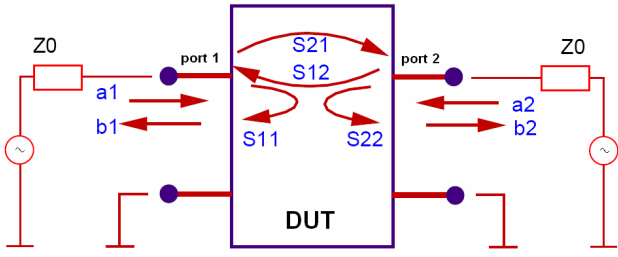


Fig. 1. Schematics of the measurement setup using a vector network analyzer (VNA) with $Z_0 = 50 \Omega$ and the PLC network as the device under test (DUT). The incident and reflected waves and the S -parameters are illustrated.

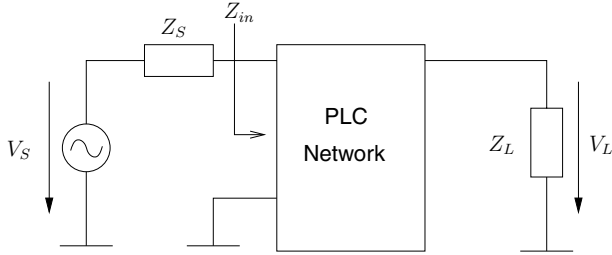


Fig. 2. Transmission over a PLC network. Transmitter source voltage V_S and impedance Z_S . Load voltage V_L and impedance Z_L .

a vector network analyzer (VNA). The measurement setup and the S -parameters are illustrated in Figure 1, where the device under test (DUT) is the power line network in the car and the reference impedance of the S -parameters is $Z_0 = 50 \Omega$.

B. Transfer Function and Input Impedance

Given the S -parameters the relevant quantities for the design of a communication system can be inferred. Considering the transmission from a source with voltage V_S and impedance Z_S to a load with impedance Z_L as shown in Figure 2, we can express the channel transfer function as

$$H = \frac{V_L}{V_S} = \frac{S_{21}(1 + \Gamma_L)(1 - \Gamma_S)}{2(1 - S_{22}\Gamma_L)(1 - \Gamma_{in}\Gamma_S)}, \quad (1)$$

where

$$\Gamma_{in} = S_{11} + \frac{S_{12}S_{21}\Gamma_L}{1 - S_{22}\Gamma_L}, \quad \Gamma_S = \frac{Z_S - Z_0}{Z_S + Z_0}, \quad \Gamma_L = \frac{Z_L - Z_0}{Z_L + Z_0},$$

are the input, source, and load reflection coefficients, respectively. If $Z_L = Z_S = Z_0$, we obtain the perhaps familiar expression

$$H = \frac{S_{21}}{2}. \quad (2)$$

The input impedance of the PLC network (see Figure 2) is given by

$$Z_{in} = Z_0 \frac{1 + \Gamma_{in}}{1 - \Gamma_{in}}. \quad (3)$$

C. Measurement Topology

The conceptual map of the power line wiring in the 2006 Pontiac Solstice is shown in Figure 3. We have considered a number of electrical components spread over different parts of the vehicle as possible communication nodes. In particular, we have used (i) the body control module (BCM), which is part of the fuse/relay box on the front passenger side of the center console, the cigarette lighter (CIG), the outside view mirror

TABLE I

MEASUREMENT NODES FOR WHICH S -PARAMETERS WERE DETERMINED.

	BCM	A/C	RearR	RearL	FrontR	FrontL	MIR	CIG
BCM								
A/C	x							
RearR	x	x						
RearL			x					
FrontR	x	x	x	x				
FrontL					x			
MIR	x	x	x	x	x			
CIG	x				x		x	

controller (MIR), and the heating ventilating air conditioning (A/C) fan button, which all are located in the passenger cabin of the car, (ii) the left (FrontL) and right (FrontR) front lights located in the engine compartment, and (iii) the left (RearL) and right (RearR) rear lights located at the rear of the car (see Figure 3). Note that the lamps (front and rear) had to be removed during the measurements to access the power line.

To obtain a complete picture of the different possible connections supported by PLC in this vehicle, measurements within and across the different compartments are necessary. Table I provides an overview of the connections for which S -parameter have been measured. Furthermore, for each pair of nodes different measurements have been taken while different electronic modules of the vehicle were activated. This will be explained in detail below. The considered frequency range is from 500 kHz to 100 MHz, which is similar to related literature [8], [10].

III. MEASUREMENT RESULTS AND DISCUSSION

In this section we present and discuss a number of measurement results. In particular, we show representative results both for transfer function and input impedance. It can be seen from equation (1) that the channel transfer function H is a function of the source and load impedances Z_S and Z_L . It is therefore preferable to show the forward transmission coefficient S_{21} , or more specifically, the insertion gain¹ $|S_{21}|$, which is independent of Z_S and Z_L , and only a function of the reference impedance $Z_0 = 50 \Omega$. According to equation (2), insertion gain and magnitude transfer function are equivalent with a constant difference of 6 dB if we choose $Z_L = Z_S = Z_0$.

A. Insertion Gains for Different Paths

First, we compare connections of different length and type. Using the terminology from [10] we consider *indirect* paths, since all paths pass through the battery. However, we also include measurements for the case that the battery is physically disconnected, which corresponds to the case of *direct* paths in [10].

Figure 4 shows the insertion gain for the three paths ‘FrontR-FrontL’, ‘FrontR-RearL’, and ‘CIG-BCM’ (see Table I) as function of frequency. For this set of measurements, the battery has been disconnected, which of course also implies that all electronic devices are turned off. We observe that the short direct link between the front lights offers a much larger insertion gain than the links crossing different compartments in the

¹Although often the term “insertion loss” is used for $|S_{21}|$, we note that the correct terminology is “gain”. Clearly, a negative gain (in dB) corresponds to an effective loss.

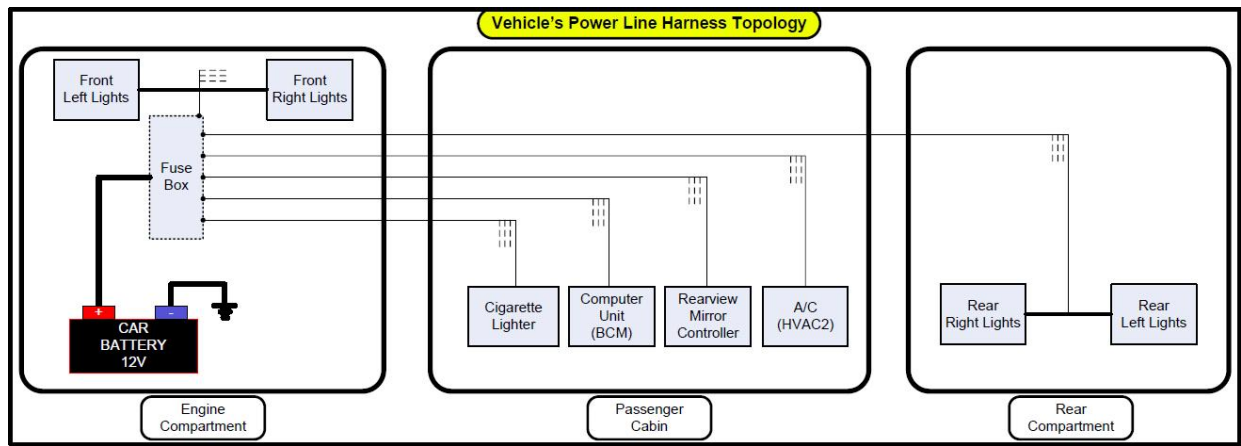


Fig. 3. Conceptual power line map of the 2006 Pontiac Solstice with the nodes considered for PLC transmission in this study.

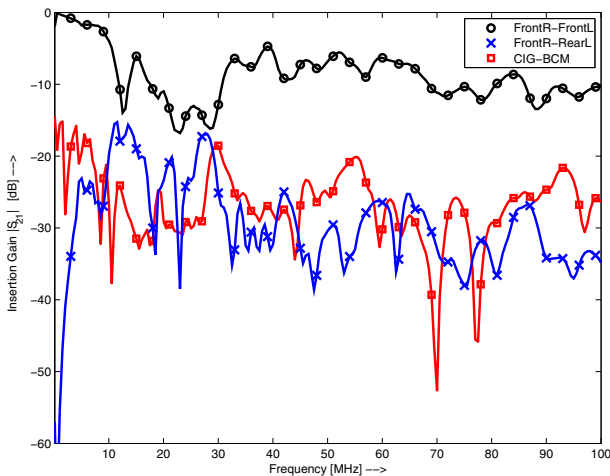


Fig. 4. Insertion gain for three different paths (see Table I). Battery disconnected.

car and having more wires branching off. The differences are consistently on the order of 20 dB. We conclude that the ‘FrontR-FrontL’ connection benefits from a relatively short length and little signal reflection. More specifically, as can be inferred from the map in Figure 3, a signal transmitted between ‘FrontR-RearL’ and ‘CIG-BCM’ likely undergoes a number of reflections along the way, which results in a log-normal shadowing effect [14] and thus smaller gains, i.e., higher attenuation. In addition, the relatively long ‘FrontR-RearL’ link suffers an additional loss compared to the ‘CIG-BCM’ link due to cable attenuation.

Figure 5 shows the insertion gains for the same links as in Figure 4, but now with all the car electronics turned on. It is important to note that by Canadian law the front low-beam lights are always running, and hence the socket of the front lamps is connected via the fuse box to the battery. Comparing the curves for ‘FrontR-FrontL’ in Figures 4 and 5 we observe that this has a notable effect on the corresponding insertion gain, which drops by about 10 dB. This is qualitatively consistent with the differences between direct and indirect paths observed in [10]. On the other hand, while the details of the curves change, no overall drop in insertion gain occurs for the ‘FrontR-RearL’ and ‘CIG-BCM’ paths.

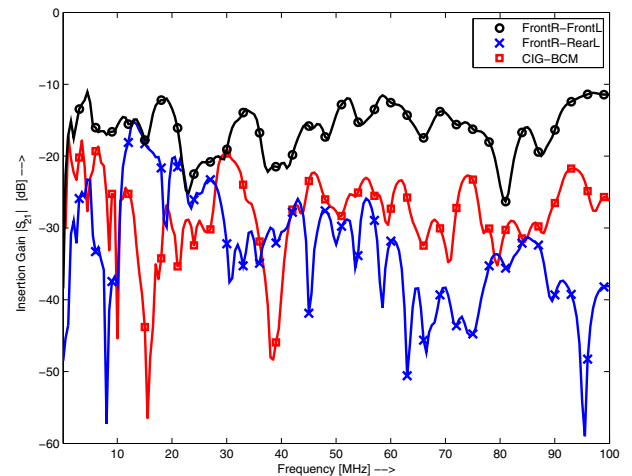


Fig. 5. Insertion gain for three different paths (see Table I). Car electronics turned on, including low-beam front lights.

B. Insertion Gain for Different Network States

Next we study the effect of the different network states. That is, we consider the effect on insertion gain of several electronic components and ignition being turned on and off. More specifically, we define the states

- ‘No battery’: The battery is removed.
- ‘No key’: The battery is connected. The car key is not in the ignition switch. Some electronic systems are powered (e.g., radio, door lock).
- ‘Key I’: The key is in the ignition switch and turned into Position I. Some electronic systems are powered (e.g., electrical windows). The low-beam front lights are off.
- ‘Key II’: The key is in the ignition switch and turned into Position II. All electronic systems including the sockets of the low-beam front lights are live. Ignition is off.
- ‘Ignition’: The ignition is on. The car idles at 1000 rpm.
- ‘2000 rpm’: The engine is driven at 2000 rpm while gear in neutral.
- Six different electronic systems are in active use (one at a time).

Figure 6 presents the insertion gain for the ‘CIG-BCM’ (top) and ‘FrontR-FrontL’ (bottom) connections, where the curves for the different network states are overlaid. For the ‘CIG-BCM’ path characterized by many branches we observe that depending on the network state notches in the insertion gain appear, which

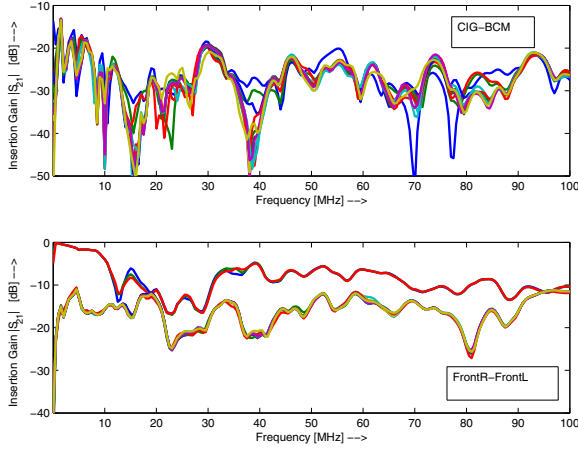


Fig. 6. Insertion gains for several network states. Top: ‘CIG-BCM’ link. Bottom: ‘FrontR-FrontL’ link. The top three curves in the bottom subplot correspond to ‘No battery’, ‘No Key’, and ‘Key I’ conditions (see description in Section III-B).

is of significance when high communication reliability is to be achieved with a relatively narrowband communication system. The short ‘FrontR-FrontL’ path is only affected by whether the low-beam front lights are connected to the battery or not, i.e., whether a direct or indirect path is experienced. This means that besides spectrally local changes as observed for the ‘CIG-BCM’ path, also global drops of insertion gains occur with changes of the network state.

C. Channel Symmetry

It has been pointed out in [15] that channel reciprocity is not equivalent to the channel being symmetric in the sense that the voltage transfer function from point A to B is identical to that from B to A. However, the authors also showed that the forward and backward transfer function are indeed identical for power line channels if source and load impedances are the same. Our measurements have confirmed this symmetry property for in-vehicle PLC channels. Figure 7 shows the difference (in dB) between forward and backward transfer function for $Z_S = Z_L$ and three sample links. We observe that they are nearly identical for all cases, with sporadic discrepancies which may be accounted to measurement effects.

D. Input Impedance

While the voltage transfer function H defined in (1) is the single important parameter for data communication assuming ideal transceivers, the input or access impedance Z_{in} of the network (see Figure 2) is another important parameter when considering practical modems. For example, if the input impedance drops below a certain threshold the transmitter modem is not able to support the required power level and the voltage at the network input will be below the nominal level.

Figure 8 shows Z_{in} from (3) as function of frequency at ‘CIG’ (top) and ‘FrontR’ (bottom) links and different network states. We observe that the impedances vary with frequency between less than 10Ω and almost 700Ω . This is the case both for the real part of Z_{in} , which is shown for ‘CIG’ in Figure 8 (top), and the magnitude impedance, which is shown for ‘FrontR’ in Figure 8 (bottom). These results are very consistent with those presented in [10, Figs. 5, 6] for different car models. A similar

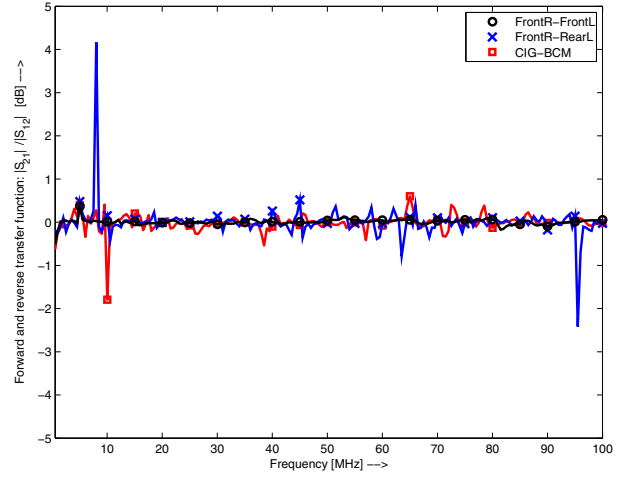


Fig. 7. Ratio between forward and reverse transfer function for different paths. ‘Key II’ state.

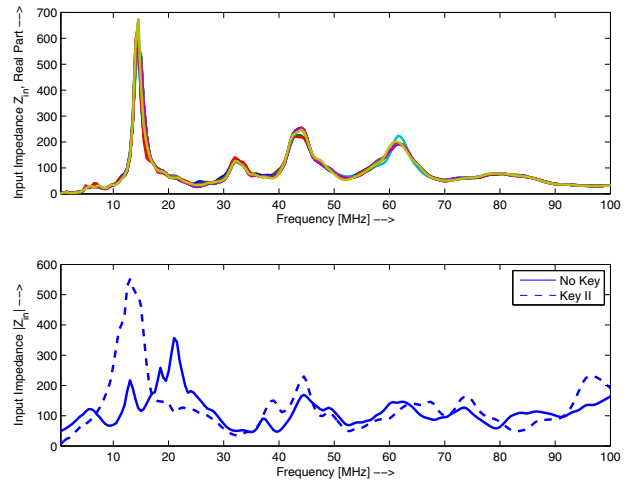


Fig. 8. Top: Input impedance (real part) at ‘CIG’ for different network states. Bottom: Input impedance (magnitude) at ‘FrontR’ for ‘No Key’ (solid line) and ‘Key II’ (dashed line).

variation of impedance levels is also known for indoor PLC channels [16]. A comparison with Figure 6 also suggests that changes of impedance and insertion gain occur simultaneously. With regards to modem design these results emphasize that impedance adaptation circuits [17] are an important design issue for in-vehicle PLC.

E. Noise Floor

It is known that the noise environment in PLC is characterized by different types of noise, among which impulsive and cyclo-stationary noise are particularly pronounced in AC PLC channels [18], [19]. Impulsive noise has also been reported for DC in-vehicle power lines and different modeling approaches have been presented in [5], [7], [11]. In order to facilitate a first evaluation about the possibility for reliable PLC communication, we have measured the background noise floor at different points in the car. We found it to be between -140 dBm/Hz and -120 dBm/Hz , which is consistent with the figures stated in e.g. [8], [9].

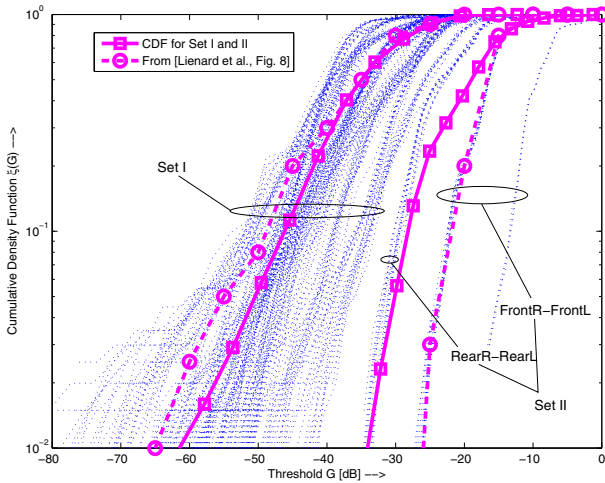


Fig. 9. Cumulative density function of insertion gains considered as random variable over frequency. Each dotted line corresponds to one link from Table I in one of the states listed in Section III-B. Solid lines: CDF for all curves in Set I and Set II, respectively. Dashed lines: CDFs from [10, Fig. 8].

IV. STATISTICAL EVALUATION AND DATA COMMUNICATION

We now move on to a statistical evaluation of the measurement results. To this end, we first consider the different links and then the different frequencies separately. Finally, guided by the results from the statistical analysis, we provide a design example for a reliable low-complexity communication system.

A. Statistics for Links

Given the transfer function H for a specific connection (see Table I) and network state (see Section III-B), we define the empirical cumulative density function (CDF) as

$$\xi(G) = \frac{|\{f : |S_{21}(f)| < G\}|}{|\{f\}|}, \quad (4)$$

where $\{f\}$ is the set of discrete frequencies at which the VNA has measured the S -parameters and its size $|\{f\}| = 200$. Figure 9 shows $\xi(G)$ as function of threshold G for the total of 211 different connections (dotted lines). Also included are two CDF curves (dashed lines) for the 500 kHz to 30 MHz range from [10, Fig. 8], which correspond to direct and indirect links as defined in [10]. It can be seen that the relatively short ‘FrontR-FrontL’ and ‘RearR-RearL’ connections stand out with relatively large insertion gains. The curves for all the remaining measurements are spread in a wide window of smaller gains. It is quite interesting to observe that the average CDFs for Set I = {‘FrontR-FrontL’, ‘RearR-RearL’} and Set 2 = {all remaining measurements} (solid lines) are very similar to those for direct and indirect links from [10], respectively. That is, even though, for example, ‘FrontR-FrontL’ in state ‘Ignition on’ is not a direct link according to [10], we observe very similar statistics for more and less favorable links as those reported in [10] for a different auto brand.

B. Statistics for Frequencies

Next, we fix the frequency and consider the statistic with regards to different links and states. Figure 10 presents the x th percentiles over all measured links and states as function of frequency for $x = [50, 10, 1]$. We observe that (i) achievable insertion gains decline considerably for small x , i.e., high

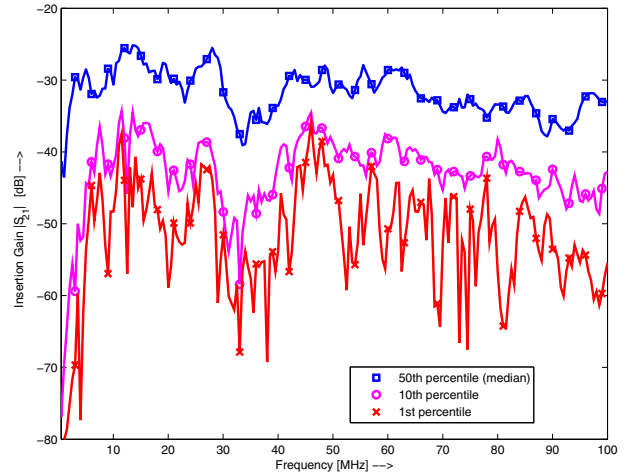


Fig. 10. 50th, 10th and 1st percentiles of insertion gains as function of frequency. Considered are all links summarized in Table I and states listed in Section III-B.

probability of staying above a threshold, and (ii) the percentiles are strongly frequency dependent. For example, the largest 50th percentile (median value) is achieved at 13.5 MHz (−25 dB), the largest 10th percentile occurs at 11.5 MHz (−34 dB), and the best 1st percentile is found at 46 MHz (−36 dB).

The results in Figure 10 make it clear that a narrowband transmission system is not able to provide sufficiently reliable connectivity. Two possibilities to improve connectivity are multihop transmission and transmission over multiple frequencies. The latter aims at frequency diversity, which could be accomplished by transmitting the same message at sufficiently widely spaced frequencies or by selecting the best of a number of possible transmit sequences. Figure 11 illustrates the possible gains in case of the latter selection combining, assuming, just for the sake of illustration, that transmission is limited to the frequency range from 20 MHz to 40 MHz and that the available n frequencies are the first n elements of [20.0, 40.0, 30.0, 25.0, 35.0, 22.5, 37.5, 27.5, 32.5] MHz. It can be seen that especially for the 1st percentile impressive gains of more than 15 dB are achievable. Furthermore, the largest fraction of the gains is accrued already with $n = 2$.

C. Example for Transmission Systems and Performance

Finally, we would like to present a transmission-system design example, which is guided by the findings above. To this end, we assume a transmit signal power spectral density (PSD) of −60 dBm/Hz and a noise PSD of $\mathcal{N}_0 = -120$ dBm/MHz (see Section III-E, [8], [9]). We note that while limits on transmit power or PSD have not been explicitly set yet, a PSD of −60 dBm/Hz has been motivated in [9].

The first, benchmark system we consider is conventional binary frequency-shift keying (FSK) with noncoherent detection. We assume narrowband FSK at a centre frequency of 20 MHz and that a 99 % connectivity is our goal. Hence, we need to be able to operate at an insertion gain of −59 dB (see Figure 11 for $n = 1$), which translates into a channel gain of −65 dB for modems with internal impedances of $Z_S = Z_L = Z_0 = 50 \Omega$ (see Equation (2)). The bit-error rate (BER) for binary FSK with noncoherent detection is given by [20, Eq. (5.4-47)]

$$P_e = \frac{1}{2} e^{-\gamma/2}, \quad (5)$$

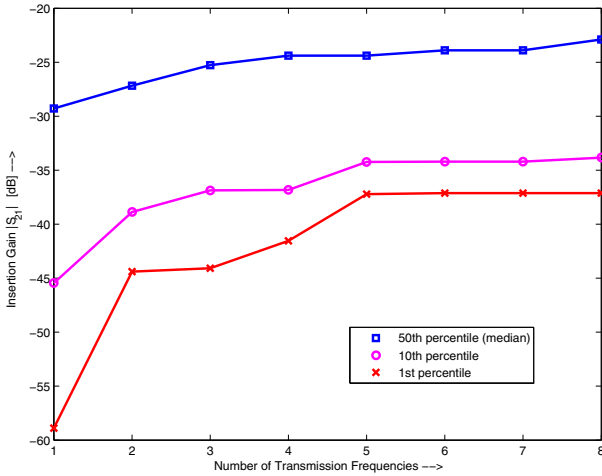


Fig. 11. 50th, 10th and 1st percentiles of insertion gains as function of the number of transmission frequencies used for selection combining. Considered are all links summarized in Table I and states listed in Section III-B. The set of frequencies are the first n elements of [20.0, 40.0, 30.0, 25.0, 35.0, 22.5, 37.5, 27.5, 32.5] MHz.

where γ is the signal-to-noise power ratio (SNR). Since

$$\gamma = \underbrace{-60 \text{ dBm/Hz}}_{\text{transmit PSD}} \underbrace{-65 \text{ dB}}_{\text{channel gain}} - \underbrace{(-120 \text{ dBm/Hz})}_{\text{noise PSD}}, \quad (6)$$

is negative, the FSK BER is close to 0.5. Even with an outer coding scheme of, say, rate 1/2, the bit-wise SNR would still be negative and thus the BER would not decrease.

An alternative transmission system, which is able to make use of frequency diversity and, in addition, is robust to narrowband and impulse noise (not considered here), is M -ary FSK with permutation trellis codes devised in [21] and investigated for PLC in [22]. As an example, we consider the rate-1/2 scheme designed for $M = 3$ [22, Table I] for transmission over $n = 3$ frequencies of [20, 30, 40] MHz. For those frequencies, we have that the 1st percentile insertion gain is -49 dB for at least two of the three frequencies (and -45 dB for one frequency as shown in Figure 11). Hence, the SNR γ is at least 5 dB at two frequencies, and thus the error-rate of a simple threshold detector for each frequency, which is given by $(Q_M(\cdot, \cdot))$ denotes the Marcum- Q -function) [23, Ch. 5]

$$P_e = \frac{1}{2} \left[e^{-\gamma/2} + 1 - Q_M(2\sqrt{\gamma}, \sqrt{\gamma}) \right], \quad (7)$$

is about 10^{-1} . Finally, consulting [21, Fig. 7] shows that the BER of the FSK permutation trellis code is then about 10^{-3} , which is an improvement by three orders of magnitude compared to the conventional FSK systems. In summary, the ($M = 3$)-FSK permutation trellis coded transmission system achieves an error rate of at least 10^{-3} for 99 % of all connections. This shows that advanced signal processing is an enabler towards high connectivity for in-vehicle PLC.

V. CONCLUSIONS

In-vehicle PLC holds great promises to enable in-vehicle communication without increasing weight, volume, or cost of the wiring harnesses. In this paper, we have provided an extensive set of channel measurements for a specific North American compact car, and we have compared these measurements with those obtained in a previous campaign for a different car. While

we could not exactly confirm the separation into direct and indirect links made in [10], we have observed a close similarity between the statistic of the transfer function for different links and network states. Furthermore, we have found that high and any-time connectivity, which is desirable for safety-critical functions, requires the use of advanced transmission techniques such as multihop or frequency diversity. Finally, we have provided a design example for a simple and robust frequency diversity transmission scheme.

REFERENCES

- [1] G. Leen and D. Heffernan, "Expanding automotive electronic systems," *IEEE Computer*, vol. 35, no. 1, pp. 88–93, Jan. 2002.
- [2] N. Navet, Y. Song, F. Simonot-Lion, and C. Wilwert, "Trends in automotive communication systems," *Proc. IEEE*, vol. 93, no. 6, pp. 1204–1223, June 2005.
- [3] F. Nouvel, G. El Zein, and J. Citerne, "Code division multiple access for an automotive network over power lines," in *IEEE Vehicular Technology Conference (VTC)*, June 1994, pp. 525–529.
- [4] Y. Maryanka, "Wiring reduction by battery power line communication," in *IEEE Seminar on Passenger Car Electrical Architecture*, June 2000, pp. 8/1–8/4.
- [5] A. Schiffer, "Statistical channel and noise modeling of vehicular dc-lines for data communication," in *IEEE Vehicular Technology Conference (VTC)*, Tokyo, Japan, May 2000, pp. 158–162.
- [6] Ford Motor Company, "Improving vehicle connectivity," online at <http://www.ford.com/innovation/automotive-technology/>, last access December 2008.
- [7] T. Huck, J. Schirmer, and K. Dostert, "Tutorial about the implementation of a vehicular high speed communication system," in *Intl. Symposium on Power Line Commun. and its Appl. (ISPLC)*, Vancouver, BC, Canada, Apr. 2005, pp. 162–166.
- [8] W. Gouret, F. Nouvel, and G. El-Zein, "Powerline communication on automotive network," in *IEEE Vehicular Technology Conference (VTC)*, Apr. 2007, pp. 2545–2549.
- [9] V. Degardin, M. Lienard, P. Degauque, and P. Laly, "Performances of the HomePlug PHY layer in the context of in-vehicle powerline communications," in *IEEE Intl. Symposium on Power Line Commun. and its Appl. (ISPLC)*, Pisa, Italy, Mar. 2007, pp. 93–97.
- [10] M. Lienard, M. Carrion, V. Degardin, and V. Degauque, "Modeling and analysis of in-vehicle power line communication channels," *IEEE Trans. Veh. Technol.*, vol. 57, no. 2, pp. 670–679, Mar. 2008.
- [11] V. Degardin, M. Lienard, P. Degauque, E. Simon, and P. Laly, "Impulse noise characterization of in-vehicle power line," *IEEE Trans. Electromagn. Compat.*, vol. 50, no. 4, pp. 861–868, Nov. 2008.
- [12] Data base of in-vehicle power line channel measurements, "<http://www.ece.ubc.ca/lampe/VehiclePLC.html>," Dec. 2008.
- [13] G. Gonzales, *Microwave transistor amplifiers: analysis and design*. Upper Saddle River, NJ, USA: Prentice-Hall, 1997.
- [14] S. Galli, "Some interesting properties of the power line channel: Towards a simplified channel model," in *submitted to the IEEE Intl. Symposium on Power Line Commun. and its Appl.*, Dresden, Germany, Mar.-Apr. 2009.
- [15] T. Banwell and S. Galli, "On the symmetry of the power line channel," in *Intl. Symposium on Power Line Commun. and its Appl.*, Malmo, Sweden, Apr. 2001.
- [16] J. Bausch, T. Kistner, M. Babic, and K. Dostert, "Characteristics of indoor power line channels in the frequency range 50-500 kHz," in *IEEE Intl. Symposium on Power Line Commun. and its Appl. (ISPLC)*, Orlando, FL, USA, Mar. 2006, pp. 86–91.
- [17] P. van Rensburg and H. Ferreira, "Design of a bidirectional impedance-adapting transformer coupling circuit for low-voltage power-line communications," *IEEE Trans. Power Delivery*, vol. 20, no. 1, pp. 64–70, Jan. 2005.
- [18] M. Zimmermann and K. Dostert, "Analysis and modeling of impulsive noise in broad-band powerline communications," *IEEE Trans. Electromagn. Compat.*, vol. 44, no. 1, pp. 249–258, Feb. 2002.
- [19] M. Katayama, T. Yamazato, and H. Okada, "A mathematical model of noise in narrowband power line communication systems," *IEEE J. Select. Areas Commun.*, vol. 23, no. 7, pp. 1267–1276, July 2006.
- [20] J. Proakis, *Digital Communications*, 3rd ed. New York: McGraw-Hill, 1995.
- [21] H. Ferreira, A. Vinck, T. Swart, and I. de Beer, "Permutation trellis codes," *IEEE Trans. Inform. Theory*, vol. 53, no. 11, pp. 1782–1789, Nov. 2005.
- [22] T. Swart, I. de Beer, H. Ferreira, and A. Vinck, "Simulation results for permutation trellis codes using M -ary FSK," in *Intl. Symposium on Power Line Commun. and its Appl. (ISPLC)*, Vancouver, BC, Canada, Apr. 2005, pp. 317–321.
- [23] J. Huber, *Course notes on Digital Communications*. University of Erlangen-Nürnberg, Germany, 1992/93.